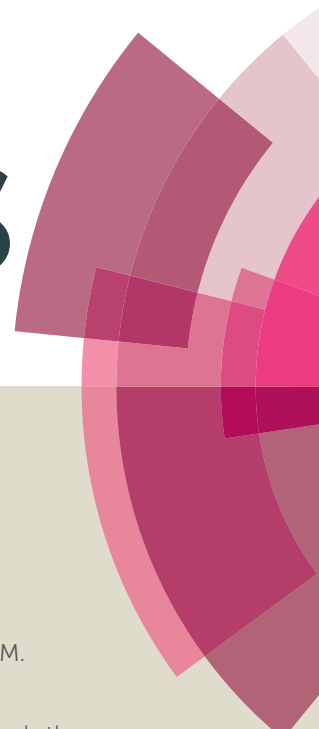


RSC Advances



This article can be cited before page numbers have been issued, to do this please use: R. Zhang, Y. Li, M. Zhang, Q. Tang and X. Zhang, *RSC Adv.*, 2016, DOI: 10.1039/C6RA01560C.



This is an *Accepted Manuscript*, which has been through the Royal Society of Chemistry peer review process and has been accepted for publication.

Accepted Manuscripts are published online shortly after acceptance, before technical editing, formatting and proof reading. Using this free service, authors can make their results available to the community, in citable form, before we publish the edited article. This *Accepted Manuscript* will be replaced by the edited, formatted and paginated article as soon as this is available.

You can find more information about *Accepted Manuscripts* in the [Information for Authors](#).

Please note that technical editing may introduce minor changes to the text and/or graphics, which may alter content. The journal's standard [Terms & Conditions](#) and the [Ethical guidelines](#) still apply. In no event shall the Royal Society of Chemistry be held responsible for any errors or omissions in this *Accepted Manuscript* or any consequences arising from the use of any information it contains.

Hypoxia-responsive drug-drug conjugated nanoparticles for breast cancer synergistic therapy

Ruilong Zhang,^{a,b,†} Yan Li,^{b,†} Miao Zhang,^{a,b} Qunwei Tang^{*a} and Xin Zhang^{*b}

^a Institute of Materials Science and Engineering, Ocean University of China, Qingdao, Shandong Province, 266100, PR China. E-mail: tangqunwei@ouc.edu.cn

^b National Key Laboratory of Biochemical Engineering, Institute of Process Engineering, Chinese Academy of Sciences, Beijing, 100190, PR China. E-mail: xzhang@ipe.ac.cn

[†] R. L. Zhang and Y. Li contributed equally to this work.

Abstract

In order to eliminate tumor, it is necessary to kill differentiated cancer cells, cancer stem cells (CSCs) and the “vascular niche” synergistically. Although nanoparticles (NPs) have been used to deliver drugs to the action sites, the inert materials with high toxicity may reduce the drug loading content and cause side-effects to kidneys and other organs in the course of degradation and excretion. Here, we reported hypoxia-responsive drug-drug conjugated NPs to deliver three drugs to kill differentiated cancer cells, CSCs and the “vascular niche” synergistically, which could selectively release the drugs to treat cells in hypoxic tumor. For this purpose, an azobenzene (AZO) bond imparting hypoxia sensitivity and specificity as crosslinker conjugated hydrophobic combretastatin A-4 (CA4) with hydrophilic irinotecan (IR) to form IR-AZO-CA4 amphiphilic molecules. These molecules self-assembled into NPs, which could encapsulate hydrophobic anti-CSCs drug cyclophosphamide (CP). The drug-drug conjugated NPs had high drug loading content. As expected, the AZO linker could be breakage under hypoxia condition and the NPs were disassembled to release drugs quickly. Confocal laser scanning microscopy (CLSM) results indicated that the IR-AZO-CA4/CP NPs could enhance the cellular uptake of drugs and the permeability of drugs to the inner of CSCs, which were benefit for tumor therapy. Furthermore, the IR-AZO-CA4/CP NPs could inhibit the migration, invasion and mammospheres formation capacity of CSCs. More importantly, only IR-AZO-CA4/CP NPs could simultaneously inhibit differentiated cancer cells, CSCs and endothelial cells without the interference on the cell under

normoxic environment. The present study suggested that the IR-AZO-CA4/CP NPs provided a promising therapeutic approach for anticancer treatment.

Keywords: hypoxia responsive, drug-drug conjugate, azobenzene bond, cancer stem cells

1. Introduction

Breast cancer is the most frequently diagnosed cancer in women according for nearly 32% of all female cancers. Despite advances in anti-cancer therapies over the years, breast cancer is still a major cause of cancer-related deaths with high recurrence, invasion and metastasis. Recent studies have suggested that cancer stem cells (CSCs) are responsible for the growth, recurrence, and metastasis of cancer.¹⁻⁵ The properties of CSCs as similar to normal stem cells, are thought to be maintained by the microenvironment of the CSCs, which is termed “niche”. Accumulating evidences show that CSCs live in a “vascular niche” that promotes their long-term growth and self-renewal.^{6,7} Hypoxia is a salient feature of solid tumors in which tumors are deprived of a supply of adequate oxygen due to their rapid growth.⁸⁻¹¹ Many experimental and clinical studies have demonstrated the tissue partial pressure of oxygen measured from tumor tissue is nearly 0 mm Hg, while it was about 30 mm Hg in normal tissue. Additionally, the phenomenon of hypoxia for CSCs is more seriously, as it has been found that CSCs are rich in hypoxia induce factor-1 α (HIF-1 α). The HIF-1 α could activate the vascular endothelial growth factor (VEGF) gene of CSCs. Therefore, the relationship between CSCs and vascular niche is interactional that the microvascular of tumor sustains CSCs with nutrients, while the CSCs secrete VEGF to trigger endothelial cells of the niche to form new capillaries.¹² From the above discussion, it seem to be a perfect tumor therapy method to target both CSCs and the vascular niche. Unfortunately, last evidences show that there is a dynamic and reversible transition between CSCs and the differentiated cancer cells in the hypoxia microenvironment of tumor. That means any survived differentiated cancer cells are tended to spontaneously and stochastically turn into CSCs, and the new CSCs have high capacity of inducing the recurrence of tumor.¹³⁻¹⁵ Hence, it's obvious that in order to eliminate tumor, it is necessary to kill the differentiated cancer cells, CSCs and the “vascular niche” synergistically.

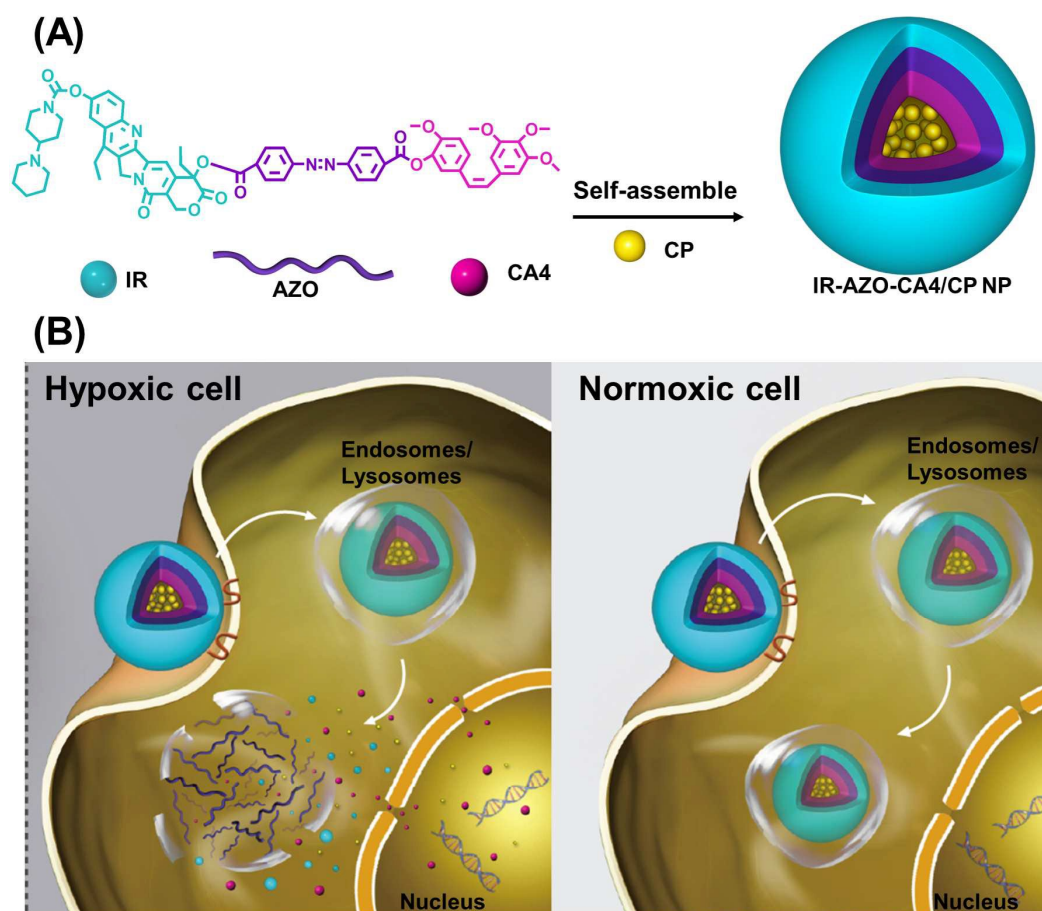
Although chemotherapy is an indispensable choice for synergistic cancer treatments, the poor bioavailability, rapid blood clearance and low accumulation of free drugs in tumors always impede

its application. Recently, Nanoparticles (NPs) have been used to deliver drugs to the action sites. However, almost all NPs themselves have no therapeutic efficacy and the drug loading contents are generally not greater than 10%.¹⁶ Even worse, most of NPs materials with high toxicity may cause side-effects to kidneys and other organs in the course of degradation and excretion. To address this challenge, it is worth looking forward that if the small molecule drugs could exhibit nanoscale characteristics by themselves without the help of NPs. Therefore, a promising drug-drug conjugate delivery system integrating both small molecule drugs and NPs could be expected to kill differentiated cancer cells, CSCs and the “vascular niche” simultaneously.

After the drug-drug conjugate delivery system accumulating in tumor site, the drug release behavior must be considered as only free drugs could kill differentiated cancer cells, CSCs and the “vascular niche” efficiently. Additionally, in order to avoid the side-effects to healthy tissues, it is ideal that the drugs were released specially in tumor. As mentioned above, hypoxia is a salient feature of solid tumors and the levels of hypoxia are more severe in tumors than normal tissues. Furthermore, nitroaromatic derivatives are hypoxia-sensitive, which could be breakage due to the reductive cleavage.¹⁷⁻²³ Of the derivatives, azobenzene (AZO) group was reported as the hypoxia-sensitive moiety and was widely used in the development of imaging agent and bioreductive prodrugs for selectively hypoxic tumor.²⁴⁻²⁶ Our previously study has developed AZO-based NPs for hydrophobic anticancer drug delivery to kill hypoxic tumor cells.²⁷ Therefore, AZO is an ideal candidate for the drug-drug conjugate.

Inspired by this, hypoxia-responsive drug-drug conjugated NPs with AZO linker were constructed in our system to kill the differentiated cancer cells, CSCs and the “vascular niche” synergistically. As shown in Scheme 1A, hydrophobic combretastatin A-4 (CA4) targeting vascular niches was conjugated with hydrophilic irinotecan (IR) inhibiting differentiated cancer cells through AZO linker to form IR-AZO-CA4 amphiphilic molecules. These IR-AZO-CA4 amphiphilic molecules could self-assemble into drug-drug conjugated NPs in an aqueous solution, which named IR-AZO-CA4 NP. Meanwhile, hydrophobic drugs cyclopamine (CP) inhibiting CSCs were encapsulated in the hydrophobic region of the drug-drug conjugated IR-AZO-CA4 NPs. So far, hypoxia-responsive drug-drug conjugated IR-AZO-CA4/CP NPs were developed, in which CA4 is one of the most potent antivasular agents that could rapidly inhibit the growth of vasculature in the tumor.²⁸ IR is a hydrophilic drug which could induces the death of the

differentiated cancer cells through DNA damage, and CP could selectively inhibit the self-renewal of CSCs through blocking the Hedgehog signaling pathway.^{29,30} The self-assembled IR-AZO-CA4/CP NPs might exhibit the following advantages: (1) the NPs with high drug loading content could deliver three drugs to the tumor site without inert materials; (2) the NPs specially released CA4, CP and IR rapidly when they were accumulated to the hypoxia zone of tumor to eliminate cancer, while the drugs could not be released in normoxic cells to avoid their toxicity to healthy tissues (Scheme 1B). Therefore, the drug-drug conjugated IR-AZO-CA4/CP NPs might open up a new avenue for synergistic cancer therapy.



Scheme 1 A) Chemical structure of IR-AZO-CA4 molecule and preparation of IR-AZO-CA4/CP NPs. B) Schematic illustration of the hypoxia-responsive drug-drug conjugated NPs in hypoxic cells and normoxic cells.

2. Experimental

2.1. Materials

4, 4'-Azobenzene dicarboxylic acid, oxalyl chloride and 1, 6-Hexanedithiol were purchased from TCI Shanghai. Triethylamine was purchased from Alfa Aesar. Irinotecan, Cyclopamine and CA4 were obtained from Dalian Meilun Biotech Co. Ltd.. MGC AnaeroPack was purchased from Mitsubishi Gas Chemical Company, Inc.. Dichloromethane was dried by calcium hydride.

2.2. Synthesis of IR-AZO-CA4

4, 4'-Azobenzene dicarboxylic acid (100 mg, 0.37 mmol) was dissolved in anhydrous CH_2Cl_2 with a drop anhydrous DMF. Oxalyl chloride (375 μL) dissolved in 10 mL anhydrous CH_2Cl_2 was added in a drop-wise manner into the 4, 4'-Azobenzene dicarboxylic acid solution. The reaction was carried out for 1 h at room temperature. The resultant solution was dried under vacuum to obtain 4, 4'-dichloroformylazobenzene.CA4 (117 mg, 0.37 mmol) and triethylamine (180 μL) were then dissolved in 10 mL anhydrous CH_2Cl_2 and added in a drop-wise manner into 4, 4'-dichloroformylazobenzene solution for 1 h. Subsequently, IR (216.8 mg, 0.37 mmol) and triethylamine (180 μL) dissolved in 10 mL anhydrous CH_2Cl_2 were added in a drop-wise manner into the solution for 1 h. The crude product was purified by column chromatography on silica gel (200-300 mesh) and eluted with 5% methanol gradient in dichloromethane. The obtained product was yellow solid and characterized by ^1H NMR, ^{13}C NMR and HR-MS.

2.3. Preparation of IR-AZO-CA4 NPs and IR-AZO-CA4/CP NPs

The IR-AZO-CA4 NPs were prepared by thin lipid film method.³¹ Briefly, the IR-AZO-CA4 molecules (5 mg) were dissolved in chloroform, the organic phase was removed at 40 °C on a rotary evaporator to obtain a thin drug film. The drug film was hydrated with 5 mL deionized water under sonication. IR-AZO-CA4 molecules (5 mg) and cyclopamine (1 mg) were dissolved in chloroform, the organic phase was removed at 40 °C on a rotary evaporator to obtain a thin drug film. The drug film was hydrated with 5 mL deionized water under sonication.

2.4. Size, zeta potential and colloidal stability of NPs measurements

Micellar size and zeta potential were determined using a Malvern Zetasizer NanoZS. Colloidal stability was measured by incubating NPs in Dulbecco's Modified Eagle Medium (DMEM) with high glucose supplemented with 10% fetal bovine serum (FBS) at 37 °C under gentle stirring. At each time point, the mean diameters of NPs were monitored by dynamic light scattering (DLS).

2.5. Drug loading efficiency and encapsulation efficiency

The encapsulation efficiency and loading content of drugs were determined using UV-spectrophotometer (IR with 405 nm, CP with 362 nm). The drug encapsulation efficiency and loading content were calculated as follows:

$$\text{Drug loading content (\%)} = W_1/W_0 \times 100\%$$

Where W_1 was the weight of drugs in NPs and W_0 was the weight of total NPs.

2.6. The morphologies of NPs, disassembled NPs

The morphologies of NPs were observed by transmission electron microscope (TEM). To examine whether these NPs could disassemble in hypoxia, we first conducted an *in vitro* assay using rat liver microsomes (75 mg mL^{-1}), which contained various reductases, and NADPH ($50 \text{ }\mu\text{M}$) as a cofactor. After treatment for 5 min, the morphology of the disassembled NPs was observed by TEM.

2.7. Cell culture

The human breast cancer cells MCF-7 and human umbilical vein endothelial cells (HUVECs) were obtained from China Academy of Medical Sciences tumor cell bank (Beijing, China). The culture medium was prepared with DMEM (Beijing North TZ-Biotech Develop, Co. Ltd. Beijing, China) supplemented with 10% heat-inactivated FBS, 50 units/mL penicillin, and 1% penicillin/streptomycin at $37 \text{ }^\circ\text{C}$ and 5% CO_2 . The cells were cultured in the incubator at $37 \text{ }^\circ\text{C}$ and in the presence of 5% CO_2 . For mammospheres culture, MCF-7 cells (1000 cells/mL) were cultured in suspension with serum-free DMEM-F12 with B27 (Invitrogen, Carlsbad, CA), 20 ng/mL EGF (BD Biosciences, Franklin Lakes, NJ), 0.4% low-endotoxin bovine serum albumin (Sangon Biotech, Shanghai, China) and 4 mg/mL insulin (Sigma-Aldrich, St. Louis, MO).

2.8. Confocal microscopy

Cellular internalization and location of Cy5-labeled NPs were tested using confocal microscopy. Briefly, the cells were incubated for 24 h in transwells. Afterwards different formulation of drugs were added to each transwell and incubated with the cells for 4 h. The cells were then detected using a Zeiss LSM80 confocal microscopy.

2.9. Wound-healing motility of MCF-7 CSCs

Wound-healing migration assay was used to study the horizontal movement of CSCs. The non-adherent spherical dissociated with 0.25% trypsin, single cell suspensions of cells were seeded onto six-well plates at 1×10^5 per well and cultured for 24 h in serum-containing medium in the incubator at 37 °C and in the presence of 5% CO₂. A single scratch wound on the confluent cells was created in each well using a sterile micropipette tip. Cells were washed thrice with PBS to remove the cell debris. After cultured the plates in an anaerobic jar 4 h at 37 °C, the remaining cells were cultured for 24 h with the same medium, followed by adding different formulations, respectively. The concentration of CP added was 0.4 mM. CSCs migrated into the scratch area as single cell from the confluent sides. The width of the scratch gap was viewed by a phase-contrast microscope at 0 and 24 h after wounding.

2.10. Cell migration inhibition assay

To quantitate vertical motility, an *in vitro* transwell migration assay was used. For transwell migration assay, CSCs suspensions were seeded in the upper compartment of the Transwell (12-well insert; 8 mm pore size; polycarbonate filter membrane; Corning Costar, Acton, MA, USA) chamber at a density of 1×10^5 cells in 0.5 mL serum-free medium. To evaluate the anti-migration ability, different formulations were added to the upper chamber, respectively. The concentration of CP added was 0.44 mM. The lower companion plate well contained DMEM plus 10% FBS. After cultured the transwell in an anaerobic jar 4 h at 37 °C, another 24 h incubation, non-migration cells were removed with cotton swabs. Cells migrated through the membrane were fixed with 4% paraformaldehyde (v/v) at room temperature, stained with crystal violet (Sigma) and counted by microscopic examination

2.11. Cell invasion inhibition assay

Cell invasion activity was measured by a transwell matrigel invasion assay. The effect of CP of different formulations on the invasiveness of CSCs were evaluated by using a Transwell chamber with Matrigel coated Membrane (12-well insert; pore size, 8 mm; Corning Costar). Each well was coated freshly with Matrigel (BD Bioscience) before the invasion assay. In this assay, CSCs (1×10^5 cells/well) were suspended in serum-free medium and applied to the matrigel followed by

filling the lower chamber with DMEM containing 10% FBS. Different formulations were added to the upper chamber, respectively. The concentration of CP added was 0.44mM. The transwell was cultured in an anaerobic jar 4 h at 37 °C, then incubated at 37 °C in 5% CO₂ incubator for 24 h and cells that did not invade through the pores were gently removed from the upper surface of the membrane by a cotton swab. Cells on the lower surface of the membrane were fixed with 4% paraformaldehyde, stained with crystal violet (Sigma) stain and counted by microscopic examination.

2.12. Inhibitory effect on MCF-7 CSCs mammospheres

Single cell suspensions of MCF-7 CSCs were seeded onto culture flask at 1.0×10^3 cells/mL and cultured in serum-free medium in the incubator at 37 °C and in the presence of 5% CO₂. The serum-free culture medium was changed every 4 days. To evaluate the inhibitory effect, MCF-7 mammospheres were treated at day 7 with different formulations, respectively (cultured the culture flask in an anaerobic jar 4 h at 37 °C first). Final concentration of CP added was 0.44 mM. The volumes of mammospheres were monitored by measuring their sizes under an inverted microscope. The major (d_{\max}) and minor (d_{\min}) diameters of each mammospheres were determined, and the volume was calculated by using the following formula: $V = (\pi \times d_{\max} \times d_{\min})/6$. The change ratio of a mammospheres volume was calculated with the formula $R = (V_{\text{day } i} / V_{\text{day } 0}) \times 100\%$, where the $V_{\text{day } i}$ is the volume of a mammospheres at the i th day after applying drug, and $V_{\text{day } 0}$ is the volume of the mammospheres prior to treatment.

2.13. Drug toxicity studies

To verify the toxicity of NPs to the tumor, we founded a non-contact co-culture model. MCF-7 cells were seeded in upper surface of transwell chambers (pore size: 0.4 μm) at a density of 2×10^4 cells/insert, and the HUVECs were seeded on the lower surface of the membrane at a density of 2×10^3 cells/insert. And the mammospheres were cultured in suspension with serum-free medium in the lower chamber. After 24 h incubation, the co-cultures were exposed to the drug treatments with PBS, IR-AZO-CA4, IR-AZO-CA4/CP and Free IR+CA4+CP. The medium should be enough to exchange through the transwell. After cultured the transwell in an anaerobic jar for 4 h at 37 °C, cultured another 48 h in serum-containing medium in the incubator at 37 °C. The three varieties

cells were collected to verify the toxicity *via* clonogenic assays.

3. Results and discussion

3.1. Synthesis and characterization of IR-AZO-CA4

To test the aforementioned hypotheses, the IR-AZO-CA4 molecule was synthesized. The synthetic routes and chemical structures of IR-AZO-CA4 were given in Fig. 1A. The formation of IR-AZO-CA4 was confirmed by ^1H NMR spectra with the characteristic peaks of IR-AZO-CA4 as indicated in Fig. 1B. Compared with the ^1H NMR of CA4, the peak at 5.55 ppm (1) related to the hydroxyl proton disappeared completely. The peak at 3.71 ppm (2) belonged to the methoxyl of CA4, while the signal of methoxyl of IR-AZO-CA4 appeared at the peak of 3.82 (2') ppm. Compared with the ^1H NMR of IR, the peak at 3.95 ppm (3) related to the hydroxyl proton disappeared completely, and the signal at 7.65 ppm (4) belonging to the pyridine ring of IR shifted to 7.42 ppm (4') in the ^1H NMR spectrum of the IR-AZO-CA4 conjugate. Furthermore, all of the chemical shift assignments to related peaks in the ^1H NMR in Fig. 1B were shown in Fig. S1 (Supporting Information). Additionally, the ^{13}C NMR was used to characterize the product and the result in Fig. S2 (Supporting Information) indicated the successful synthesis of IR-AZO-CA4. The mass and molecular formula of the obtained product were determined by HR-MS (positive, Bruker, USA), in which m/z 1138.24 $[\text{M} + \text{H}]^+$ and 1155.24 $[\text{M} + \text{NH}_4]^+$ were consistent with the molecular mass of $\text{C}_{65}\text{H}_{64}\text{N}_6\text{O}_{13}$ ($M=1137.24$) for IR-AZO-CA4 (Fig. S3, Supporting Information). Those results demonstrated that IR-AZO-CA4 was successfully synthesized.

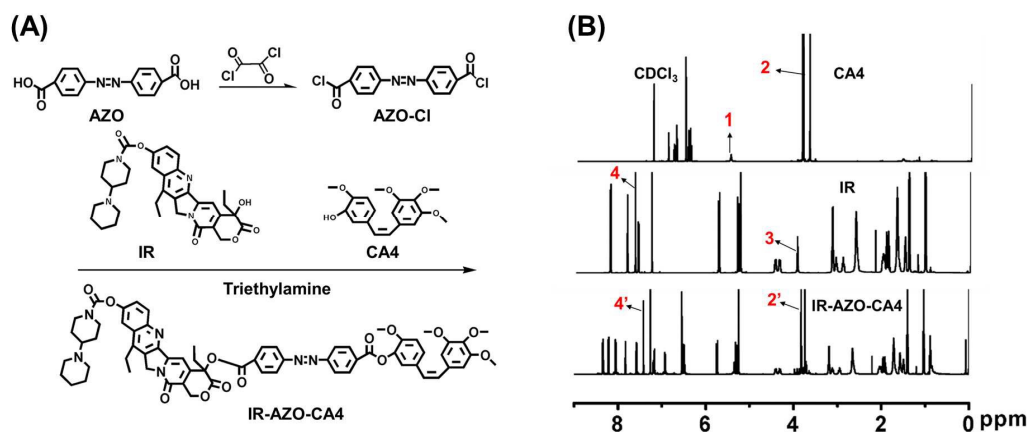


Fig. 1 A) Synthetic route of the IR-AZO-CA4. B) ^1H NMR spectra of IR-AZO-CA4 (600 MHz, CDCl_3).

3.2. The characterization of IR-AZO-CA4 NPs

After the successful synthesis of the IR-AZO-CA4 molecule, the drug-drug conjugated NPs were prepared and the physicochemical properties of NPs were evaluated in the following studies. Hydrophobic drug CP was chosen as anti-CSCs drugs encapsulated in NPs. The average diameter of IR-AZO-CA4 NPs were about 195.9 ± 8.3 nm determined by DLS studies. IR-AZO-CA4 NPs encapsulated CP with a hydrodynamic diameter of particle of 205.9 ± 6.9 nm, were little bigger than IR-AZO-CA4 NPs due to the encapsulation of CP in hydrophobic region (Fig. 2A). The zeta potential of all NPs was low (Fig. S4), which was benefit for the serum stability of NPs. The loading content of IR-AZO-CA4/CP NPs was detected by UV-spectrophotometer. As shown in Fig. 2B, NPs with high loading content of 15.2%, 42.3% and 22.7% for CP, IR and CA4, respectively.

The *in vitro* colloidal stability of IR-AZO-CA4 NPs and IR-AZO-CA4/CP NPs were investigated in DMEM containing 10% FBS. As shown in Fig. 2C, for 72 h incubation, no significant size changes were observed for IR-AZO-CA4 NPs and IR-AZO-CA4/CP NPs. These results suggested that IR-AZO-CA4 NPs and IR-AZO-CA4/CP NPs had better colloidal stability in FBS environment. The release of CP from IR-AZO-CA4/CP NPs in physiological environment was studied in PBS (pH 7.4) at 37 °C. The result in Fig. 2D showed that 8.4% of CP was released in 4 days. This result indicated that IR-AZO-CA4/CP NPs were sufficiently stable under physiological conditions. Taken together, these findings were important because colloidal stability in FBS and low release of drug in physiological environment for any NPs determined the successful delivery of drugs to tumor. These two features prevented particles aggregation and premature burst drug release from circulatory system, which prolonged the NPs residence time in the body and enhanced the NPs accumulation in tumor *via* enhanced permeation and retention (EPR) effect.³²

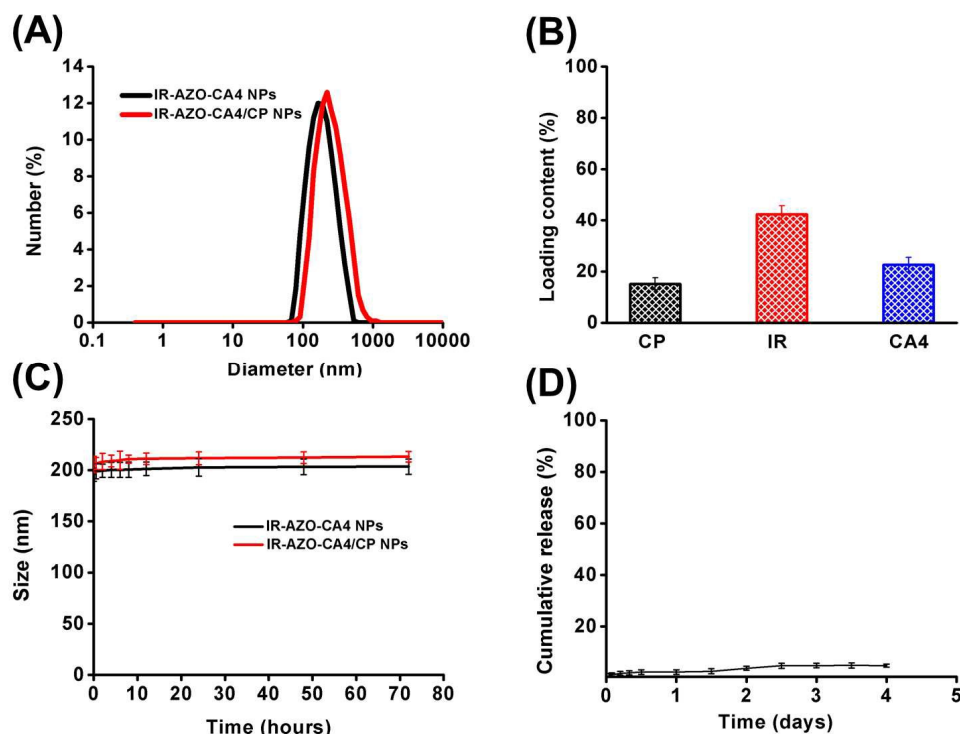


Fig. 2 A) The size distribution of NPs detected by DLS. B) The drugs loading content detected by UV-spectrophotometer. C) The stability of IR-AZO-CA4 and IR-AZO-CA4/CP NPs in DMEM with 10% FBS (n=3). D) Release profiles of CP from IR-AZO-CA4/CP NPs in PBS (pH 7.4) at 37 °C (n=3).

3.3. Drug release of NPs under hypoxia environment

Owing to the introduction of hypoxia-sensitive AZO bonds, the IR-AZO-CA4 NPs and IR-AZO-CA4/CP NPs were expected to disassemble quickly when they were exposed to reductive enzymes under conditions of hypoxia³³. After adding NADPH (50 μM) as a cofactor for the reductases to the yellow IR-AZO-CA4 NPs (2 mg mL^{-1}) (Fig. 3A a1) in the presence of rat liver microsomes (75 $\mu\text{g mL}^{-1}$), the yellow solution slowly turned colorless and yellow precipitate appeared in the centrifuge tube (Fig. 3A a2). Meanwhile, the IR-AZO-CA4/CP NPs aqueous solution (2 mg mL^{-1}) (Fig. 3A a3 and a4) exhibited the same phenomenon. These results suggested that the AZO bond was cleavage under reductive hypoxic condition (75 mg mL^{-1} rat liver microsomes with 50 μM NADPH as cofactor), which resulted in the disassembling of NPs and releasing of drugs. To further confirm the disassembled NPs under reductive hypoxic condition (75 mg mL^{-1} rat liver microsomes with 50 μM NADPH as cofactor), the morphologies of IR-AZO-CA4 NPs and IR-AZO-CA4/CP NPs before and after treatment with NADPH and rat

liver microsomes were observed by transmission electron microscope (TEM). The IR-AZO-CA4 (Fig. 3A a1) and IR-AZO-CA4/CP (Fig. 3A a3) NPs were spherical structure with unimodal size distribution before treatment, while these two NPs were disassembled after treatment under hypoxia (75 mg mL⁻¹ rat liver microsomes with 50 μM NADPH as cofactor) (Fig. 3A a2 and a4). Furthermore, as shown in Fig. S5, IR-AZO-CA4 molecule had a broad absorption band centered 450 nm, which was the typical adsorption for the AZO chromophore. After treating with 75 mg mL⁻¹ rat liver microsomes with 50 μM NADPH as cofactor, the absorption range was disappeared due to the cleavage of AZO bond of IR-AZO-CA4 molecule. The cleavage of AZO bond mechanism of IR-AZO-CA4 molecule was shown in Fig. 3B.³⁴ In addition, the size of IR-AZO-CA4 NPs and IR-AZO-CA4/CP gradually became bigger as shown in Fig S6. Taken together, IR-AZO-CA4 NPs and IR-AZO-CA4/CP NPs were disassembled and triggered the fast release of encapsulated CP, free CA4 and free IR under condition of reductive enzymes in hypoxia.

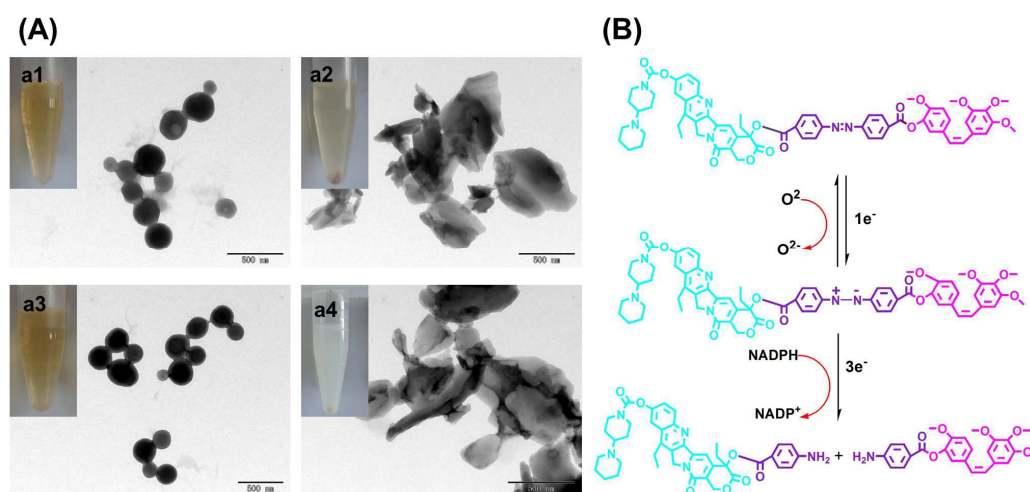


Fig. 3 A) The TEM image of NPs and image of NPs in aqueous solution before and after treatment with rat liver microsomes (75 μg mL⁻¹) and NADPH (50 μM) as a cofactor. a1. IR-AZO-CA4 NPs before treatment; a2. IR-AZO-CA4 NPs after treatment; a3. IR-AZO-CA4/CP NPs before treatment; a4. IR-AZO-CA4/CP NPs after treatment. Bar = 500 nm. B) The cleavage of AZO bond mechanism of IR-AZO-CA4 molecule.

3.4. *In vitro* distribution studies of IR-AZO-CA4/Cy5 NPs

The cellular uptake of NPs were studied by confocal laser scanning microscopy (CLSM), and Cy5

(red) instead of CP and IR (blue) were used as fluorescence probe. MCF-7 cells were cultured with IR-AZO-CA4/Cy5 NPs, IR-AZO-CA4 NPs and free drugs for 4 h before observation. As shown in Fig. 4A, the IR-AZO-CA4/Cy5 NPs could be internalized quickly than free drugs with the largest mean fluorescence intensity (MFI) of Cy5 and IR, especially for hydrophobic Cy5 (Fig. 4C). To further confirm whether IR-AZO-CA4/Cy5 NPs could enhance the permeability, the distribution of Cy5 and IR in MCF-7 mammospheres were observed in three dimension. As shown in Fig. 4B, most of the IR were on the surface of MCF-7 mammospheres for free drug and there was almost no Cy5 fluorescence. Interestingly, the fluorescence of IR and Cy5 for IR-AZO-CA4/Cy5 NPs were distributed in the whole of mammospheres. The quantified results in Fig. 4D further confirmed this conclusion that the MFI of Cy5 and IR for IR-AZO-CA4/Cy5 NPs was much larger than free Cy5 and IR. The results indicated that the IR-AZO-CA4/Cy5 NPs could facilitate the permeability of drugs, especially the hydrophobic drugs to the inner of CSCs, which was benefit for tumor therapy.

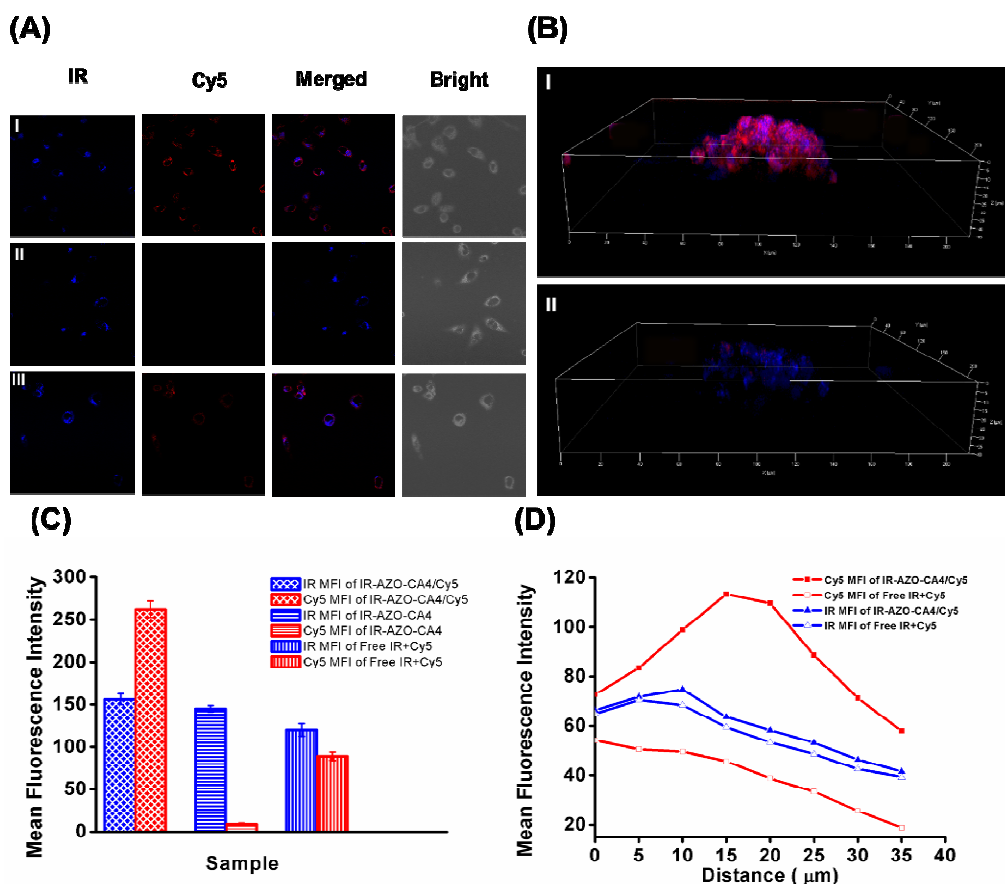


Fig. 4 A) CLSM images of IR-AZO-CA4/CP NPs in MCF-7 cells for 4 h. I: IR-AZO-CA4/Cy5, II:

IR-AZO-CA4, III: Free IR+Cy5. The excitation wavelengths were 405 nm and 630 nm for IR and Cy5, respectively. B) Three dimension of CLSM images of MCF-7 mammospheres. I: IR-AZO-CA4/Cy5, II: Free IR+Cy5. C) Mean Fluorescence Intensity of IR and Cy5 in MCF-7 cells quantified from Fig. 4A. I: IR-AZO-CA4/Cy5, II: IR-AZO-CA4, III: Free IR+Cy5 D) Mean Fluorescence Intensity of IR and Cy5 in MCF-7 mammospheres quantified from Fig. 4B.

3.5. Inhibition effect on wound-healing, migration and invasion of MCF-7 CSCs

Due to the fact that CSCs played a significant role in tumor recurrence and metastasis, wound-healing, migration and matrigel invasion were investigated to evaluate the inhibitory effects of NPs on the malignant behavior of CSCs. Fig. 5A showed the invasion with a single scratch by a pipette tip on the adherent MCF-7 CSCs and the wound-healing response after applying different NPs formulations. When the adherent CSCs were wounded, self-renewed and scratch wound were healed quickly. The wound width of control at 24 h was only 44.5% (inhibition rate) of the width at 0 h, with a healing rate of 55.5% after treated with PBS. IR-AZO-CA4 NPs without CP had little effect with a healing rate of 35.4%, as the drugs of IR and CA4 had weak effect on CSCs. In comparison, IR-AZO-CA4/CP NPs exhibited the strongest inhibitory effect on the wound-healing response of CSCs with a healing rate of 7.7% due to their better cellular uptake, which is even better than free CP (with a healing rate of 8.7%).

Fig. 5B showed the inhibitory effect of NPs on the migration of CSCs. Obvious inhibition on the migration was observed in CSCs treated with IR-AZO-CA4/CP NPs compared with other groups. Fig. 5C showed the influence of NPs on invasion of CSCs. IR-AZO-CA4 NPs had no remarkable inhibitory effects on CSCs invasion, and free CP decreased the number of invading cells. As expected, IR-AZO-CA4/CP NPs exhibited the strongest inhibitory effect on the invasion of CSCs. Those results indicated that the cell migration and invasion were efficiently inhibited by the intracellular delivery CP of IR-AZO-CA4/CP NPs.

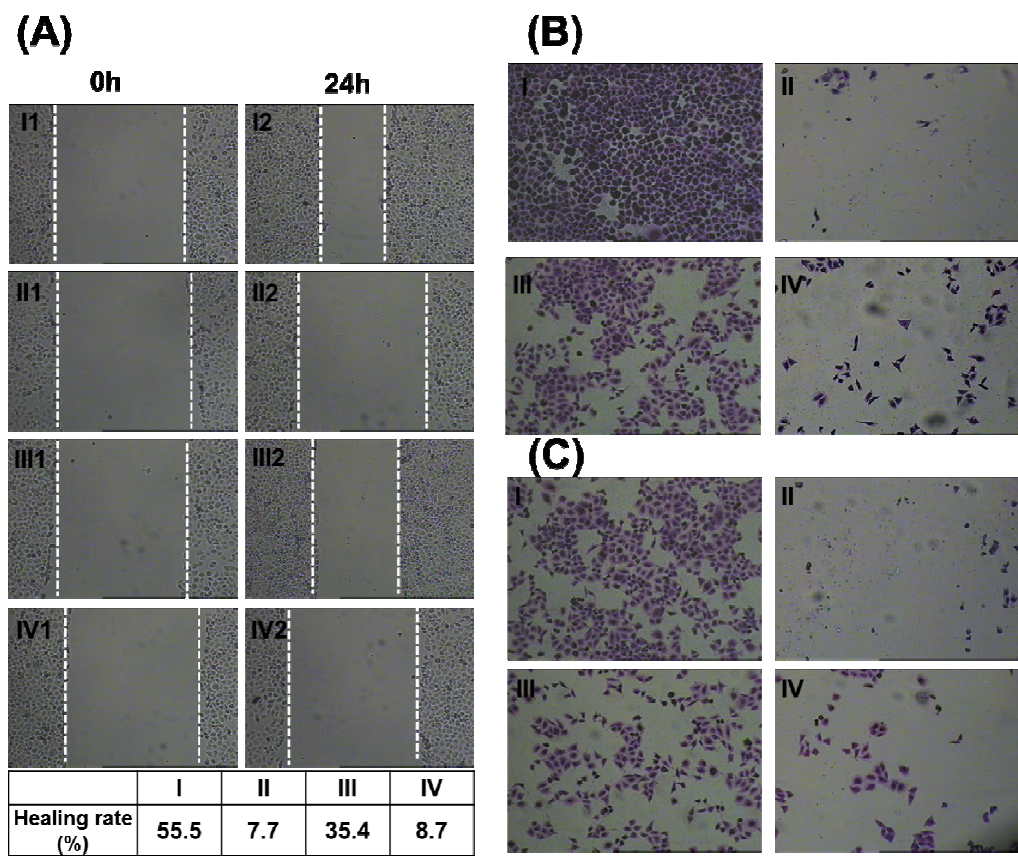


Fig. 5 The influence of IR-AZO-CA4/CP NPs on migratory and invasion properties of CSCs. A) Invasive wound by a single scratch by a pipettor tip on the adherent MCF-7 CSCs and the wound-healing response after applying different formulations at 0 h and 24 h, respectively. B) The influence of different formulations on migration of MCF-7 CSCs. Magnification: 10 \times . C) The influence of different formulations on invasion of MCF-7 CSCs, Magnification: 10 \times . I: PBS, II: IR-AZO-CA4/CP NPs, III: IR-AZO-CA4 NPs, IV: Free CP.

3.6. Inhibition of IR-AZO-CA4/CP NPs on MCF-7 mammospheres fomulation

We further employed tumorsphere culture to explore the CSCs subpopulation from human breast cancer lines MCF-7 produced spheroid after *in vitro* culture for 1 week in serum-free medium. To evaluate the inhibitory effects of NPs on the mammospheres formation, mammospheres were treated at day 7 with PBS, IR-AZO-CA4 NPs, IR-AZO-CA4/CP NPs, free IR, free CA4 and free CP, respectively. Fig. 6A showed the effect of different formulations treatment on the mammospheres formation capacity of CSCs. IR-AZO-CA4 NPs, free IR and free CA4 treatment

conserved the ability of CSCs to form mammospheres to 112-150%, while free CP treatment resulted in the reduction of the mammospheres size to 34%. It was noteworthy that treatment with IR-AZO-CA4/CP NPs exhibited the strongest inhibitory effect of CSCs mammospheres to 22%. Those results suggested that IR-AZO-CA4/CP NPs could significantly inhibit the growth of CSCs subpopulations due to their better cellular uptake and permeability.

3.7. *In vitro* cytotoxicity

To evaluate the anticancer efficiency of IR-AZO-CA4 NPs and IR-AZO-CA4/CP NPs on differentiated cancer cells, CSCs and vascular niches (using human umbilical vein endothelial cells as model, HUVECs), the cellular viability assays were tested under normoxic and hypoxic conditions, respectively. As shown in Fig. 6B and Fig. 6C, the cell survival ratio reduced to 17.9% and 10.6% for differentiated MCF-7 cancer cells and HUVEC, respectively, after treating with IR-AZO-CA4 NPs under hypoxia environment (anaerobic jar), while the NPs had almost no effect on MCF-7 CSCs (Fig. 6D). In comparison, the IR-AZO-CA4/CP NPs formulations could efficiently inhibit the three kinds of cells simultaneously under hypoxia (anaerobic jar), with the cell viability of 14.2%, 10.6% and 23% for MCF-7 cancer cells, HUVECs and CSCs, respectively (Fig. 6D). It was worth noting that the inhibitory effect of the NPs on cells was negligible under normoxic condition, which was very different from free drugs. Taken together of these three results, it demonstrated that not only the IR-AZO-CA4/CP NPs could inhibit the proliferation of differentiated cancer cells, CSCs and endothelial cells of vascular niches (HUVECs) simultaneously, but also could avoid cytotoxicity to healthy tissues in normoxic environment.

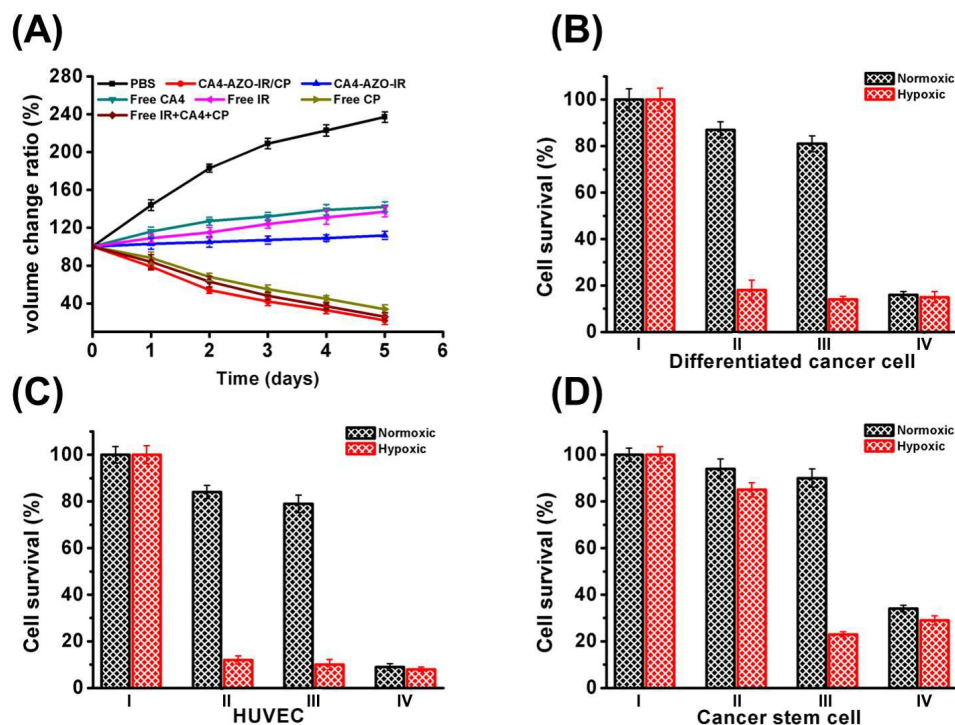


Fig. 6 A) Inhibitory effect on the growth of CSCs mammospheres after applying different formulations. Cytotoxicity of different formulations on B) MCF-7 differentiated cancer cells, C) HUVEC and D) MCF-7 CSCs under normoxic and hypoxic conditions. I : PBS; II : IR-AZO-CA4 NPs; III : IR-AZO-CA4/CP NPs; IV: Free IR+CA4+CP. Data are presented as the means \pm SD, $n = 3$.

4. Conclusions

In summary, we successfully developed hypoxia-responsive IR-AZO-CA4/CP NPs, which could significantly induce the apoptosis and prohibit the proliferation of differentiated cancer cells, CSCs and vascular niches (HUVECs) synergistically. The NPs were stable in PBS environment and had almost no premature burst drug released from circulatory system. As expected, the AZO linker could be breakage under hypoxia condition (75 mg mL⁻¹ rat liver microsomes with 50 μ M NADPH as cofactor) and the NPs were disassembled to release drugs quickly. The CLSM results indicated that the IR-AZO-CA4/CP NPs could enhance the cellular uptake of drugs and the permeability of drugs to the inner of CSCs, which were benefit for tumor therapy. The migration, invasion and mammospheres formation capacity of CSCs were significantly inhibited by IR-AZO-CA4/CP NPs. More importantly, only IR-AZO-CA4/CP NPs could simultaneously

inhibit differentiated cancer cells, CSCs and HUVECs without the interference on the cell viability under normoxic environment. The present study suggested that the IR-AZO-CA4/CP NPs provided a promising therapeutic approach for cancer treatment.

Acknowledgements

This work was financially supported by the National Natural Science Foundation of China (315220023, 51373177), the National High Technology Research and Development Program (2014AA020708), the Instrument Developing Project of the Chinese Academy of Sciences (YZ201313), the “Strategic Priority Research Program” of the Chinese Academy of Sciences (XDA09030301-3), the BeiJing National Science Foundation (Grant No.Z141100000214010). All procedures involving experimental animals were performed in accordance with protocols approved by the Institutional Animals Care and Use Committee of Peking University.

References

- 1 B. J. Morrison, C. W. Schmidt, S. R. Lakhi, B. A. Reynolds and J. A. Lopez, Breast cancer cells: implications for therapy of breast cancer, *Breast Cancer Res*, 2008, **10**, 1-8.
- 2 H. Cleves, The cancer stem cell: premises, promises and challenges, *Nat Med*, 2011, **17**, 313-319.
- 3 T. Reya, S. J. Morrison, M. F. Clarke, and I. L. Weissman, Stem cells, cancer, and CSCs, *Nature*, 2001, **414**, 105-111.
- 4 C. J. Emmanuelle, G. Christophe, I. Flora, W. Julien, C. Nathalie, F. Pascal, H. Min-Hee, E. D. Mark, M. Florence, D. Julie, B. Marthy, V. Patrice, X. Luc, B. François, S. Giorgio, D. Gabriela, B. Daniel and W. Max S, Breast cancer cell lines contain functional cancer stem cell with metastatic capacity and a distinct molecular signature, *Cancer Res*, 2009, **69**, 1302-1313.
- 5 F. Li, B. Tiede, J. Massague and Y. Kang, Beyond tumorigenesis: CSCs in metastasis, *Cell Res*, 2007, **17**, 3-14.
- 6 C. Calabrese, H. Poppleton, M. Kocak, T. L. Hogg, C. Fuller, B. Hamner, E. Young Oh, M. W. Gaber, D. Finklestein, M. Allen, A. Frank, I. T. Bayazitov, S. S. Zakharenko, A. Gajjar, A. Davidoff and R. J. Gilbertson, A perivascular niche for brain tumor stem cell, *Cancer Cell*, 2007, **11**, 69-82.
- 7 Z. J. Yang and R. J. Wechsler-Reya, Hit'em where they live: targeting the cancer stem cell niche, *Cancer Cell*, 2007, **11**, 3-5.
- 8 M. W. Moyer, Targeting hypoxia brings breath of fresh air to cancer therapy, *Nat Med.*, 2012, **18**, 636-637.
- 9 W. R. Wilson and M. P. Hay, Targeting hypoxia in cancer therapy, *Nat Rev Cancer*, 2011, **11**, 393-410.
- 10 A. L. Harris, Hypoxia-a key regulatory factor in tumor growth, *Nat Rev Cancer*, 2002, **2**, 38-47.
- 11 J. M. Brown and W. R. Wilson, Exploiting tumor hypoxia in cancer treatment, *Nat Rev Cancer*, 2004, **4**, 437-447.
- 12 R. K. Ambasta, A. Sharma and P. Kumar, Nanoparticle mediated targeting of VEGFR and cancer stem cell for cancer therapy, *Vascular Cell*, 2011, **3**, 1-9.

- 13 D. Klevebring, G. Rosin, R. Ma, J. Lindberg, K. Czene, J. Kere, I. Fredriksson, J. Bergh and J. Hartman, Sequencing of breast cancer stem cell populations indicates a dynamic conversion between differentiation states in vivo, *Breast Cancer Res*, 2014, **16**, 72-72.
- 14 C. L. Chaffer, I. Brueckmann, C. Scheel, A. J. Kaestli, P. A. Wiggins, L. O. Rodrigues, M. Brooks, F. Reinhardt, Y. Suc, K. Polyak, L. M. Arendt, C. Kuperwasser, B. Bierie and R. A. Weinberg, Normal and neoplastic nonstem cells can spontaneously convert to a stem-like state, *Proc Natl Acad Sci USA*, 2011, **108**, 7950-7955.
- 15 P. B. Gupa, C. M. Fillmore, G. Z. Jiang, S. D. Shapira, K. Tao, C. Kuperwasser and E. S. Lander, Stochastic state transitions give rise to phenotypic equilibrium in populations of cancer cells, *Cell*, 2011, **146**, 633-644.
- 16 Y. Shen, E. Jin, B. Zhang, C. J. Murphy, M. Sui, J. Zhao, J. Wang, J. Tang, M. Fan, E. V. Kirk and W. J. Murdoch, Prodrugs Forming High Drug Loading Multifunctional Nanocapsules for Intracellular Cancer Drug Delivery, *J. AM. CHEM. SOC.* 2010, **132**, 4259-4265.
- 17 Y. Liu, Y. Xu, X. Qian, J. Liu, L. Shen, J. Li and Y. Zhang, Novel fluorescent markers for hypoxic cells of naphthalimides with two heterocyclic side chains for bioreductive binding, *Bioorg. Med. Chem.*, 2006, **14**, 2935-2941.
- 18 L. Cui, Y. Zhong, W. Zhu, Y. Xu, Q. Du, X. Wang, X. Qian and Y. Xiao, A new prodrug-derived ratiometric fluorescent probe for hypoxic: high selectivity of nitroreductase and imaging in tumor cell, *Org. Lett.*, 2011, **13**, 928-931.
- 19 K. Xu, F. Wang, X. Pan, R. Liu, J. Ma, F. Kong and B. Tang, High selectivity imaging of nitroreductase using a near-infrared fluorescence probe in hypoxic tumor, *Chem. Commun.*, 2013, **49**, 2554-2556.
- 20 H. Komatsu, H. Harada, K. Tanabe, M. Hiraoka and S. Nishimoto, Indolequinone-rhodol conjugate as a fluorescent probe for hypoxic cells: enzymatic activation and fluorescence properties, *Med Chem Comm*, 2010, **1**, 50-53.
- 21 S. Zhang, M. Hosaka, T. Yoshihara, K. Negishi, Y. Iida, S. Tobita and T. Takeuchi, Phosphorescent Light-Emitting Iridium Complexes Serve as a Hypoxic-Sensing Probe for Tumor Imaging in Living Animals, *Cancer Res.*, 2010, **70**, 4490-4498.
- 22 E. Nakata, Y. Yukimachi, H. Kariyazono, S. Im, C. Abe, Y. Uto, H. Maezawa, T. Hashimoto, Y. Okamoto and H. Hori, Design of a bioreductively-activated fluorescent pH probe for tumor

- hypoxic imaging, *Bioorg. Med. Chem.*, 2009, **17**, 6952-6958.
- 23 Z. Li, X. Li, X.Gao, Y. Zhang, W. Shi and H. Ma, Nitroreductase Detection and Hypoxic Tumor Cell Imaging by a Designed Sensitive and Selective Fluorescent Probe, 7-[(5-Nitrofuran-2-yl)methoxy]-3Hphenoxazin-3-one, *Anal. Chem.*, 2013, **85**, 3926-3932.
- 24 J. Rao and A. Khan, Enzyme sensitive synthetic polymer micelles based on the azobenzene motif, *J. Am. Chem. Soc.*, 2013, **135**, 14056-14059.
- 25 F. Perche, S. Biswas, T. Wang, L. Zhu and V. P. Torchilin, Hypoxic-targeted siRNA delivery, *Angew. Chem., Int. Ed.*, 2014, **53**, 3362-3366.
- 26 T. Thambi, V. G. Deepagan, H. Y. Yoon, H. S. Han, S. H. Kim, S. Son, D. G. Jo, C. H. Ahn, Y. D. Suh, K. Kim, I. C. Kwon, D. S. Lee, J. H. Park, Hypoxia-responsive polymeric nanoparticles for tumor-targeted drug delivery, *Biomaterials*, 2014, **35**, 1735-1743.
- 27 H. Liu, R. Zhang, Y. Niu, Y. Li, C. Qiao, J. Weng, J. Li, X. Zhang, Z. Xiao and X. Zhang, Development of hypoxia-triggered prodrug micelles as doxorubicin carriers for tumor therapy, *RSC adv*, 2015, **5**, 20848-20857.
- 28 G. M. Tozer, C. Kanthou, C. S. Parkins and S. A. Hill. The biology of the combretastatins as tumour vascular targeting agents. *Int J Exp Pathol*, 2002, **83**, 21-38.
- 29 Y. Pommier. Topoisomerase I inhibitors: camptothecins and beyond. *Nat. Rev. Cancer*, 2006, **6**, 789–802.
- 30 C. Zhao, A. Chen, C. H. Jamieson, M. Fereshteh, A. Abrahamsson, J. Blum, H. Y. Kwon, J. Kim, J. P. Chute, D. Rizzieri, M. Munchhof, T. VanArsdale, P. A. Beachy and T. Reya. Hedgehog signaling is essential for maintenance of cancer stem cells self-renewal, and tumorigenicity. *Curr Biol*, 2007, **17**, 165-172.
- 31 T. Wei, J. Liu, H. L Ma, Q. Cheng, Y. Y. Huang, J. Zhao, S. D. Huo, X. D. Xue, Z. C. Liang, X. J. Liang, Functionalized nanoscale micelles improve drug delivery for cancer therapy *in vitro* and *in vivo*, *Nano Lett.*, 2013, **13**, 2528-2534.
- 32 A. Vanessa, P. H. Adriana, L. E. Magda, T. L. Madeline and R. Carlos, Effect of surface charge on the colloidal stability and in vitro uptake of carboxymethyl dextran-coated iron oxide nanoparticles, *J Nanopart Res*, 2013, **15**, 1874-1888.
- 33 W. Piao, S. Tsuda, Y. Tanaka, S. Maeda, F. Y. Liu, S. Takahashi, Y. Kushida, T. Komatsu, T. Ueno, T. Terai, T. Nakazawa, M. Uchiyama, K. Morokuma, T. Nagano and K. Hanaoka,

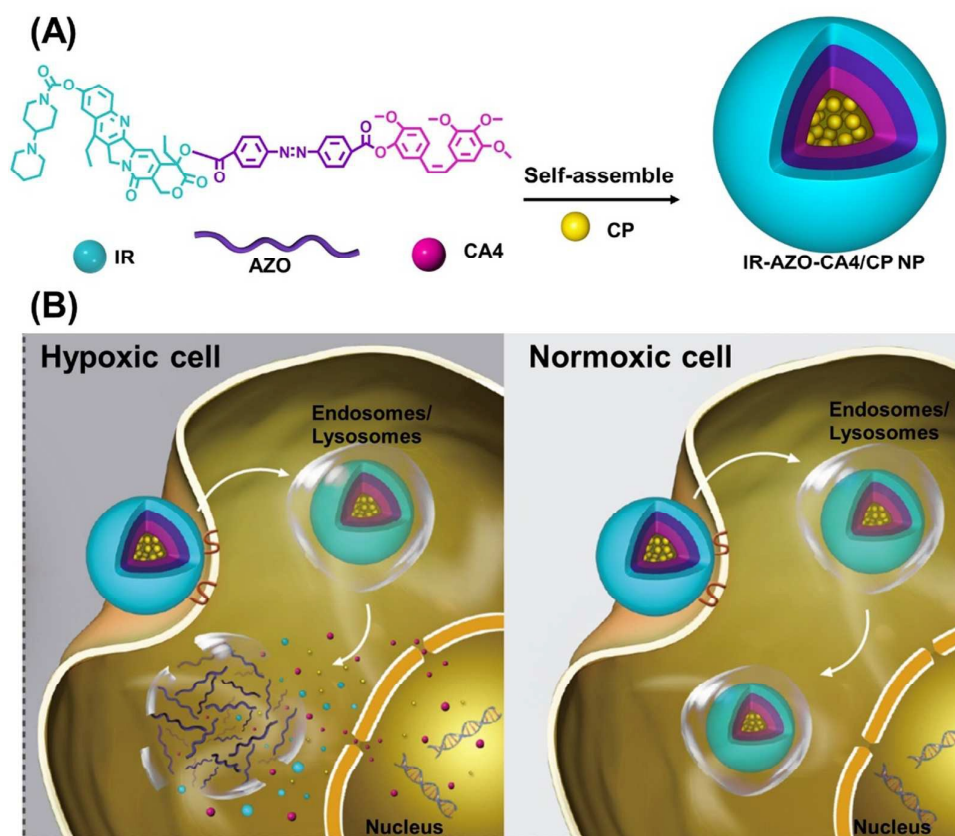
Development of Azo - Based Fluorescent Probes to Detect Different Levels of Hypoxic, *Angew. Chem., Int. Ed.*, 2013, **52**, 13028-13032.

- 34 U. A. Hrozhyk, S. V. Serak, N. V. Tabiryan, L. Hoke, D. M. Steeves, B. Kimball and G. Kedziora, Systematic Study of Absorption Spectra of Donor–Acceptor Azobenzene Mesogenic Structures, *Mol. Cryst. Liq. Cryst.*, 2008, **489**, 257-272.

Abstract

In order to eliminate tumor, it is necessary to kill differentiated cancer cells, cancer stem cells (CSCs) and the “vascular niche” synergistically. Although nanoparticles (NPs) have been used to deliver drugs to the action sites, the inert materials with high toxicity may reduce the drug loading content and cause side-effects to kidneys and other organs in the course of degradation and excretion. Here, we reported hypoxia-responsive drug-drug conjugated NPs to deliver three drugs to kill differentiated cancer cells, CSCs and the “vascular niche” synergistically, which could selectively release the drugs to treat cells in hypoxic tumor. For this purpose, an azobenzene (AZO) bond imparting hypoxia sensitivity and specificity as crosslinker conjugated hydrophobic combretastatin A-4 (CA4) with hydrophilic irinotecan (IR) to form IR-AZO-CA4 amphiphilic molecules. These molecules self-assembled into NPs, which could encapsulate hydrophobic anti-CSCs drug cyclophosphamide (CP). The drug-drug conjugated NPs had high drug loading content. As expected, the AZO linker could be breakage under hypoxia condition and the NPs were disassembled to release drugs quickly. Confocal laser scanning microscopy (CLSM) results indicated that the IR-AZO-CA4/CP NPs could enhance the cellular uptake of drugs and the permeability of drugs to the inner of CSCs, which were benefit for tumor therapy. Furthermore, the IR-AZO-CA4/CP NPs could inhibit the migration, invasion and mammospheres formation capacity of CSCs. More importantly, only IR-AZO-CA4/CP NPs could simultaneously inhibit differentiated cancer cells, CSCs and endothelial cells without the interference on the cell under normoxic environment. The present study suggested that the IR-AZO-CA4/CP NPs provided a promising therapeutic approach for anticancer treatment.

Keywords: hypoxia responsive, drug-drug conjugate, azobenzene bond, cancer stem cells



Scheme 1 A) Chemical structure of IR-AZO-CA4 molecule and preparation of IR-AZO-CA4/CP NPs. B) Schematic illustration of the hypoxia-responsive drug-drug conjugated NPs in hypoxic cells and normoxic cells.